Effective medium theory of the space-charge region electrostatics of arrays of nanoscale junctions

Vijaya Kumar Gurugubelli and Shreepad Karmalkar

Citation: J. Appl. Phys. **119**, 024507 (2016); doi: 10.1063/1.4939763
View online: http://dx.doi.org/10.1063/1.4939763
View Table of Contents: http://aip.scitation.org/toc/jap/119/2
Published by the American Institute of Physics

Effective medium theory of the space-charge region electrostatics of arrays of nanoscale junctions

Vijaya Kumar Gurugubelli[a] and Shreepad Karmalkar
Department of Electrical Engineering, Indian Institute of Technology Madras, Chennai 600036, India

(Received 19 October 2015; accepted 29 December 2015; published online 13 January 2016)

We develop an Effective Medium Theory for the electrostatics of the Space-Charge Region (SCR) of Schottky and *p-n* junctions in arrays of nanofilms (NFs), nanowires (NWs), and nanotubes (NTs) in a dielectric ambient. The theory captures the effects of electric fields in both the semiconductor, i.e., NF/NW/NT, and the dielectric media of the array. It shows that the depletion width and the screening length characterizing the SCR tail in the array correspond to those in a bulk junction with an effective semiconductor medium, whose permittivity and doping are their weighted averages over the cross-sectional areas of the semiconductor and dielectric; the shapes of the cross-sections are immaterial. Further, the reverse bias $1/C^2$-V behavior of junctions in NF/NW/NT arrays is linear, as in bulk junctions, and is useful to extract from measurements the built-in potential, effective doping including the semiconductor-dielectric interface charge, and NF/NW/NT length. The theory is validated with numerical simulations, is useful for the experimentalist, and yields simple formulas for nano-device design which predict the following. In the limiting case of a single sheet-like NF, the junction depletion width variation with potential drop is linear rather than square-root (as in a bulk junction). In arrays of symmetric silicon *p-n* junctions in oxide dielectric where NF/NW thickness and separation are 5% and 100% of the bulk depletion width, respectively, the junction depletion width and the screening length are scaled up from their bulk values by the same factor of ~2 for NF and ~10 for NW array. © *2016 AIP Publishing LLC*.
[http://dx.doi.org/10.1063/1.4939763]

I. INTRODUCTION

Schottky and *p-n* junctions in arrays of nanofilms (NFs) or nanowires (NWs) or nanotubes (NTs), like the ones shown in Figs. 1(a) and 1(b), are of practical interest in upcoming nanoscale devices. Arrays of NW/NT junctions find applications in photovoltaics,[1,2] Light Emitting Diodes (LEDs),[3–6] photodetectors,[7–9] etc. Array of NF junctions appears at the source and drain contacts in FINFETs,[10] and in devices made in layers of two-dimensional materials; for example, recently, a stack of alternating layers of graphene and hexagonal boron nitride insulator has been grown for potential device applications.[11] Moreover, in the study of low-dimensional effects, as one moves from bulk to a single NF/NW/NT, an array of NFs/NWs/NTs in a dielectric medium serves as an intermediate situation.[12]

The behavior of junctions is governed by the Space-Charge Region (SCR) electrostatics. The SCR consists of a region near the junction completely depleted of mobile carriers and a partially depleted tail beyond this region. A knowledge of the depletion width, i.e., the SCR width approximating the SCR to be fully depleted of mobile carriers, is useful for estimating the junction characteristics such as charge/capacitance/field versus voltage and breakdown voltage. On the other hand, a knowledge of the SCR tail width is useful for accurate estimation of the onset of phenomena which depend upon electrostatic interaction between adjacent junctions of the device.[13]

Recently, we analyzed the SCR electrostatics of Schottky junctions in arrays of NWs/NTs,[14] and lateral *p-n* junctions in single NFs.[15] The present paper expands and unifies this analysis into an Effective Medium Theory (EMT) for the SCR electrostatics of Schottky and *p-n* junctions in arrays of NFs/NWs/NTs (see Figs. 1(a) and 1(b)). The theory captures the effects of the electric field in both the semiconductor, i.e., NF/NW/NT, and dielectric media of the array. It shows that the depletion width and the screening length characterizing the SCR tail in the array correspond to those in a bulk junction with an effective semiconductor medium whose permittivity and doping are their weighted averages over the cross-sectional areas of the semiconductor and dielectric.

The main result of our EMT theory is as follows. Consider the *p*-side SCR of a uniformly doped *bulk* *p*-type Schottky or *p-n* junction. The depletion width W_{pB} (p for *p*-side and B for bulk) for a potential drop V_p and the Debye length L_{Dp} characterizing the SCR tail beyond the depletion width are given by[16,17]

$$W_{pB} = \sqrt{\frac{2\epsilon_s V_p}{qN_A}} \quad \text{and} \quad L_{Dp} = \sqrt{\frac{\epsilon_s V_t}{qN_A}}, \tag{1}$$

where ϵ_s is the semiconductor permittivity, q is the electronic charge, N_A is the doping, and V_t is the thermal voltage; L_{Dp} is the screening length derived from the potential distribution in the SCR under linear screening. The SCR tail width is a fraction of W_{pB} and is on the order of L_{Dp}. Note that V_p includes both applied and built-in voltages. When the bulk

[a]Electronic mail: vkgurugubelli@gmail.com

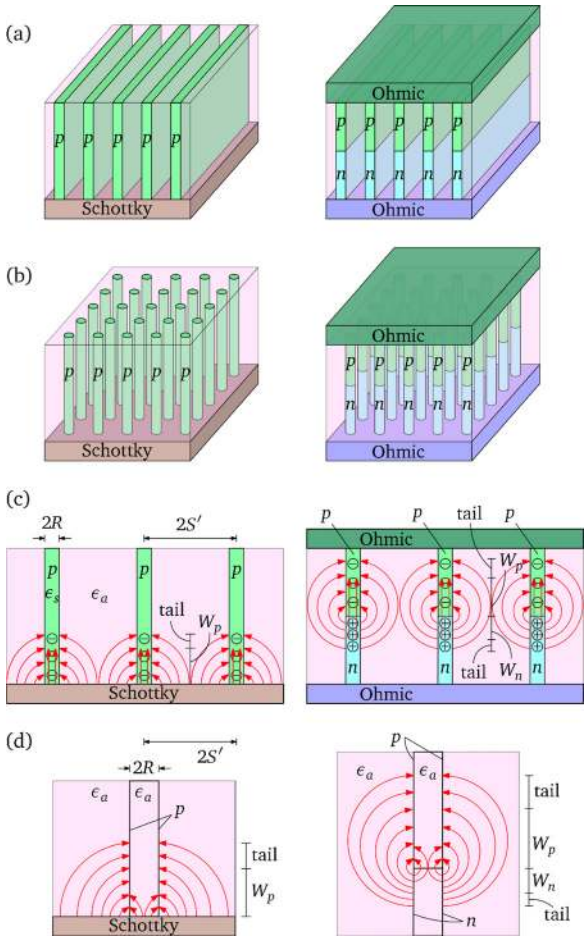

FIG. 1. Schottky and *p-n* junctions in an array of nanofilms (a) and nanowires (b). The cross-sections of junctions in nanofilm and nanowire arrays are identical; (c) shows these and the field lines. A nanotube array appears like (b), except that the wires are hollow, and has the field lines shown in (d).

semiconductor is replaced by an array of semiconductor NFs/NWs/NTs (see Fig. 1), the field in the dielectric ambient surrounding the NF/NW/NT increases the depletion width and screening length by several times.[14,15] The EMT developed in this paper yields the *p*-side depletion width W_p and screening length L_{Ap} (*A* for Array) in the array as

$$W_p = \sqrt{\frac{2\epsilon_{emt}V_p}{qN_{Aemt}}} \quad \text{and} \quad L_{Ap} = \sqrt{\frac{\epsilon_{emt}V_t}{qN_{Aemt}}}, \tag{2}$$

where

$$\epsilon_{emt} = \frac{\epsilon_s A_s + \epsilon_a A_a}{A_s + A_a} \quad \text{and} \quad N_{Aemt} = \frac{N_A A_s + 0 \times A_a}{A_s + A_a}, \tag{3}$$

and A_s and A_a are the cross-sectional areas of the semiconductor NF/NW/NT and the ambient dielectric, respectively. Interpretation of these results for nanofilms and nanowires is straight forward; semiconductor-dielectric interface charge σ_f, if any, is accounted for by regarding N_A in Eq. (3) as the net doping due to volume doping and an amount obtained by distributing σ_f uniformly over the film/wire thickness. For nanotubes, we regard ϵ_s and A_s as the permittivity and cross-sectional area of the medium inside the tube, respectively, and N_A as the doping obtained by distributing the surface doping uniformly over the tube thickness. Analogous results apply for an *n*-type Schottky junction and for the *n*-side SCR of a *p-n* junction, i.e., we can obtain the *n*-side depletion widths W_{nB} and W_n and the screening lengths L_{Dn} and L_{An} by replacing V_p and N_A by *n*-side potential drop V_n and doping N_D, respectively. In ultra-thin NFs/NWs, the built-in voltage component of V_p and V_n should be calculated including the quantum confinement effects. We validate our theory by comparing it with accurate self-consistent numerical simulations. Although we develop our theory using the widely prevalent configuration of square arrays of cylindrical NWs/NTs, we show that our theory works for NW/NT arrays of other configurations too.

II. STRUCTURAL PARAMETERS AND QUALITATIVE UNDERSTANDING OF SCR ELECTROSTATICS

Based on the field lines shown in Figs. 1(c) and 1(d), it can be inferred that the SCR electrostatics of these junctions depends on the NF/NW/NT thickness/diameter $2R$, inter-film/wire/tube separation $2S'$, ambient permittivity ϵ_a, and σ_f, in addition to the parameters that affect a bulk junction, namely, N_A, N_D, ϵ_s, and potential drop $V_d = V_p + V_n = V_{bi} - V_a$, where V_a is the applied voltage and V_{bi} is the built-in potential. The bulk values of V_{bi} = work function difference φ_{ms} in a Schottky junction and $V_t \log(N_A N_D/n_i^2)$ in a *p-n* junction apply to NFs/NWs also, as long as the NFs/NWs are not ultra-thin to be affected by quantum confinement, which increases the V_{bi} above the bulk value as discussed later in Section VIII. Below we present a qualitative understanding of the SCR electrostatics modeled in the present work.

We consider Schottky junctions for explanation. Similar explanations hold good for *p-n* junctions. Fig. 2(a) shows the simulated equilibrium space-charge density in bulk, NF array, and NW array junctions. The corresponding electric field distributions appear in Fig. 2(b). The simulations are performed in Sentaurus TCAD[18] by self-consistently solving the Poisson's equation and drift-diffusion transport equations.[17] Fig. 2(a) reveals that the depletion and SCR tail widths increase from bulk to NF to NW. This is due to the fact that there is no surrounding flux in bulk, and that the surrounding flux due to E_x in NF and E_r in NW, that uses up some of the space-charge, is more in NW than in NF. Since only the remaining space-charge can cause the fall of the axial electric field E_z, the rate of fall of E_z decreases from bulk to NF to NW as shown in Fig. 2(b). Since the potential drop $\int E_z dz$ is same for all the distributions, the peak E_z reduces and SCR width increases from bulk to NF to NW. Correspondingly, the extent of SCR width over which the normal field (E_r in NW and E_x in NF) terminates increases from NF to NW (see Fig. 2(b)).

Our present work models this variation of depletion width and SCR tail width.

III. EQUATIONS AND APPROXIMATIONS

We first consider NF and NW arrays. We then apply the results of NW array to treat an NT array, realizing that, from an electrostatic view point, an NT array is analogous to an

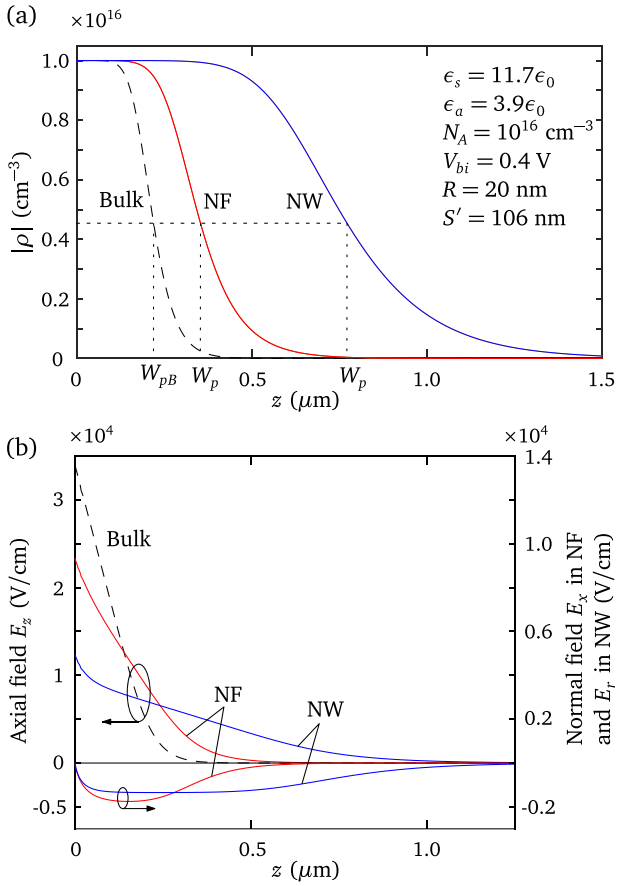

FIG. 2. Simulated equilibrium distributions of space-charge (a) and electric field (b) in Schottky junctions realized in bulk silicon, and in arrays of silicon NFs/NWs in SiO_2 ambient.

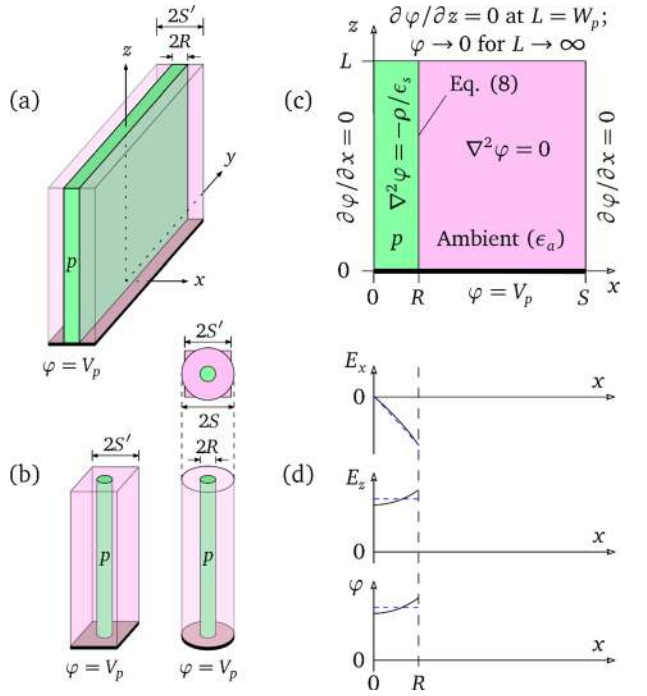

FIG. 3. (a) The simplified nanostructure of the NF array of Fig. 1(a). (b) The simplified nanostructure of the NW array of Fig. 1(b). (c) Equations and boundary conditions for analyzing the NF structure of (a). (d) Actual (solid lines) and approximate (dashed lines) distributions of the field and potential inside the NF of (a). (c) and (d) apply to the NW structure of (b) by replacing x by r, and Eq. (8) by Eq. (10).

NW array with $\epsilon_s = \epsilon_a$, and zero space-charge but non-zero interface charge.[14] Note that the analysis of the Schottky junction also applies to an array wherein the Schottky metal is replaced by a heavily doped bulk semiconductor of opposite polarity to that of the array.

Without any loss of generality, we regard the semiconductor part of the Schottky junction to be p-type, and the p-side of the p-n junction to be lightly doped relative to the n-side. Considering the symmetry of the arrays shown in Figs. 1(a) and 1(b), to model their SCR electrostatics, it suffices to analyze the electrostatics of the simplified nanostructures shown in Figs. 3(a) and 3(b), which are the p-side of the unit or Wigner-Seitz cells of the array. Each simplified nanostructure is a single NF/NW/NT surrounded by a dielectric medium with dimensions governed by $2S'$. In the case of NW/NT (see Fig. 3(b)), the cuboidal dielectric of cross-sectional area $4S'^2$ surrounding the cylindrical NW/NT is transformed to a cylinder of same cross-sectional area,[14,19] i.e., radius $S = (2/\sqrt{\pi})S'$. The NF/NW/NT stands on an equipotential plane $\varphi = V_p$ at $z = 0$, and the normal field over the outer surface of the dielectric is zero.

We point out the approximations involved in the above simplification and their rationale. The equipotential condition on the plane $z = 0$ is accurate for a Schottky junction array and a p-n junction array with $N_A = N_D$, but is an approximation for a p-n junction array with $N_A \neq N_D$. Recently Ref. 15 showed that this equipotential plane approximation works well for a single NF p-n junction with $N_A \neq N_D$. This approximation is even more valid for an array with finite S considered in this paper, since a single NF is equivalent to an NF in an array with $S \to \infty$ and the percentage variation in φ over S would be smaller for finite S than for $S \to \infty$. The cuboidal to cylindrical transformation of the dielectric brings in cylindrical symmetry. The preservation of the cross-sectional area in this transformation and the condition of zero normal field on the outer surface of the cylindrical dielectric are essential to conserve the ambient electric flux responsible for the nanoscale effects. Reference 19 mentions the preservation of the cross-sectional area as a means of preserving the areal density of NWs alone.

Various features of the SCR electrostatics can be modeled based on the potential distribution φ as a function of V_p, N_A, and R. Such a function can be obtained from a solution of the Poisson's equation

$$\nabla^2\varphi = \begin{cases} -\rho/\epsilon_s & \text{for} \quad 0 \le x, r \le R \\ 0 & \text{for} \quad R < x, r \le S, \end{cases} \tag{4}$$

where ρ is the space-charge density. Poisson's equation is adequate and Schrödinger's equation need not be considered in this solution, since quantum effects, if any, alter the density of states and hence V_{bi} alone, and not the function itself. Hence, we develop our theory from a solution of the Poisson's equation and point out the modifications required in V_{bi} to include quantum effects.

Our recent works[14,15] showed based on numerical simulations that the field and potential distributions over the

NF/NW thickness can be approximated in a simple manner. We introduce these approximations considering an NF (see Fig. 3(c)), where the horizontal x-axis is along the junction or the equipotential plane, and the vertical z-axis is along the middle of the NF. As long as $R \lesssim W_{pB}$, for $x \leq R$, we can make the following three approximations regarding the field and potential distributions (see Fig. 3(d)): E_x varies linearly with x from $E_x = 0$ at $x = 0$ (note that $E_x = 0$ at $x = 0$ due to symmetry); E_z is constant with x because the variation in E_z over R is much smaller than the magnitude of E_z; φ is constant with x for similar reasons. We emphasize that our linear approximation of E_x is not the derivative of the constant φ approximation, but rather, an approximation of the derivative of the actual φ. The above approximations apply to NWs by replacing x by r, since the horizontal x-axis is the r-axis and the vertical z-axis is the NW axis. In addition, in NFs, $E_y \approx 0$ because the NF dimension in y direction is $\gg W_p$; an NF array in which this dimension is comparable with W_p is better treated as a one-dimensional array of NWs.

The boundary condition over the plane away from the equipotential plane (see Fig. 3(c)), to be employed for solving the Laplace's equation for φ, has been explained in our prior works.[14,15] To derive φ over the SCR tail, which extends to long distances away from the equipotential plane, we employ $\varphi \to 0$ for $z \to \infty$. However, this boundary condition is not suitable to obtain a solution for φ under the depletion approximation of ρ, which yields a simple analytical formula for W_p. For this purpose, we employ the alternative boundary condition $\partial\varphi/\partial z = 0$ at $z = W_p$, i.e., no field line crosses the plane $z = W_p$, which is a direct consequence of the complete depletion approximation. Note that, even though $\varphi = 0$ at $(x, z) = (0, W_p)$, the boundary condition $\varphi = 0$ at $z = W_p$ cannot be employed here, because the potential cannot remain constant over the entire plane $z = W_p$ due to the existence of a field component along this plane.

IV. SOLUTION METHODOLOGY

Since simple approximations are possible for the field and potential distributions inside the NF/NW, we find it convenient to work with the electric field, and hence write the Poisson's equation in the form of Gauss's law. Using the approximations in the Gauss's law yields an equation for the field distribution along the NF/NW-dielectric interface. This equation provides the fourth boundary condition together with the other three shown in Fig. 3(c) to solve the Poisson's equation outside the NF/NW, where the Poisson's equation reduces to the Laplace's equation and can be solved using separation of variables. This solution is combined with the constant φ approximation to obtain the potential distribution inside the NF/NW. We consider the case of NF and NW in turn.

Consider the case of the NF. Refer to Fig. 3(c) showing the equations and boundary conditions. Inside the NF, $E_y \approx 0$ and hence the Gauss's law is

$$\frac{\partial E_x}{\partial x} + \frac{\partial E_z}{\partial z} = \frac{\rho}{\epsilon_s}. \tag{5}$$

Putting together the linear E_x vs x approximation and the continuity of the normal electric flux across the boundary $x = R$ where we may have σ_f, we get

$$\frac{\partial E_x(x,z)}{\partial x} \approx \frac{E_x(R^-,z)}{R} = -\frac{1}{R}\frac{\epsilon_a}{\epsilon_s}\frac{\partial\varphi(R^+,z)}{\partial x} - \frac{\sigma_f}{R\epsilon_s}. \tag{6}$$

Similarly, putting together the constant E_z versus x approximation and the continuity of the tangential electric field across the boundary $x = R$, we get

$$\frac{\partial E_z(x,z)}{\partial z} \approx \frac{\partial E_z(R^-,z)}{\partial z} = -\frac{\partial^2\varphi(R^+,z)}{\partial z^2}. \tag{7}$$

Substitution of Eqs. (6) and (7) into Eq. (5) leads to

$$\frac{1}{R}\frac{\epsilon_a}{\epsilon_s}\frac{\partial\varphi(R^+,z)}{\partial x} + \frac{\partial^2\varphi(R^+,z)}{\partial z^2} = -\frac{\left(\rho + \sigma_f/R\right)}{\epsilon_s}. \tag{8}$$

Using this equation governing the field distribution at $x = R^+$ as the fourth boundary condition (see Fig. 3(c) for the other three), we solve the Laplace's equation as shown later to obtain $\varphi(R^+, z)$. Since the potential is continuous across the NF-dielectric interface and approximately constant over the NF thickness, $\varphi(R^+, z)$ also happens to be the $\varphi(x, z)$ over the NF thickness.

The case of the NW can be treated in an analogous manner. Inside the NW, the Gauss's law is

$$\frac{\partial E_r}{\partial r} + \frac{E_r}{r} + \frac{\partial E_z}{\partial z} = \frac{\rho}{\epsilon_s}. \tag{9}$$

Based on the linear E_r, constant E_z, and constant φ approximations over r for $0 \leq r < R$, and noting that a linear E_r vs r implies $E_r/r = \partial E_r/\partial r$ in Eq. (9), we obtain the following equation analogous to Eq. (8) of NF

$$\frac{2}{R}\frac{\epsilon_a}{\epsilon_s}\frac{\partial\varphi(R^+,z)}{\partial r} + \frac{\partial^2\varphi(R^+,z)}{\partial z^2} = -\frac{\left(\rho + 2\sigma_f/R\right)}{\epsilon_s}. \tag{10}$$

As in the case of the NF, this equation is used to solve the Laplace's equation to obtain $\varphi(R^+, z)$, which also happens to be the $\varphi(r, z)$ over the NW thickness.

Our models for NFs and NWs are derived assuming $\sigma_f = 0$ for simplicity. However, as shown in our previous work,[15] they can be readily used for non-zero $\sigma_f = qN_f$ by replacing the doping levels N_A and N_D in model expressions by effective doping levels

$$\begin{aligned} N_{Aeff} &= N_A - N_f/R\,;\; N_{Deff} = N_D + N_f/R \quad \text{for} \quad \text{NFs} \\ N_{Aeff} &= N_A - 2N_f/R\,;\; N_{Deff} = N_D + 2N_f/R \quad \text{for} \quad \text{NWs}. \end{aligned} \tag{11}$$

Thus, interface charge is modeled as a change in volume doping by an amount obtained by distributing the interface charge uniformly over the film/wire thickness. This amount turns out to be $2N_f/2R = N_f/R$ for NFs (the factor 2 is because the film has two surfaces) and $N_f \times 2\pi R/\pi R^2 = 2N_f/R$ for NWs. Eq. (11) should be used wherever N_A and N_D appear in the formulas, including in the V_{bi} expression.

It is of interest to note the limitations of an alternate solution methodology based on conformal mapping. First, it is applicable only to a 2D situation, so that it cannot be applied directly to treat an NW/NT array, wherein the potential variation is 3D. Second, even when applicable, it does not always give simple results. Thus, in the case of NF arrays, which have a 2D potential variation, it has enabled a solution only for a single NF of zero thickness (see Refs. 20–22), and even for this special case, the solution is more complicated than our solution. If the mapping functions employed in Refs. 20–22 are extended either to a single NF of nonzero thickness or to an NF array, the transformed boundaries become irregular, making the mapping ineffective. For these reasons, conformal mapping cannot yield a unified analytical model for arrays of NWs, NTs, and NFs.

V. JUNCTION DEPLETION WIDTH

A. Nanofilm array

Application of the solution methodology presented in Section IV to an NF array results in the following implicit equation for W_p (see Appendix A 1)

$$\frac{W_p}{W_{pB}} \approx \sqrt{1+\frac{\epsilon_a}{\epsilon_s}\frac{\tanh\left[\pi(S-R)/2W_p\right]}{\pi R/2W_p}}, \tag{12}$$

where W_{pB} is given by Eq. (1).

For small $\pi(S-R)/2W_p$, we have $\tanh[\pi(S-R)/2W_p] \approx \pi(S-R)/2W_p$, so that Eq. (12) yields the following closed-form equation:

$$W_p \approx \zeta W_{pB} \quad \text{where} \quad \zeta = \sqrt{1+\frac{\epsilon_a}{\epsilon_s}\left[\frac{S}{R}-1\right]}. \tag{13}$$

We have found that this equation is within 10% error for

$$\frac{W_p}{R} \geq \frac{\pi}{\sqrt{2}}\left(\frac{S}{R}-1\right). \tag{14}$$

For large $\pi(S-R)/2W_p$, we have $\tanh[\pi(S-R)/2W_p] \approx 1$, so that Eq. (12) yields the following closed-form equation derived in Ref. 15 for a single NF junction

$$\frac{W_p}{W_{pB}} \approx \frac{1}{\pi}\frac{\epsilon_a}{\epsilon_s}\frac{W_{pB}}{R}+\sqrt{\left(\frac{1}{\pi}\frac{\epsilon_a}{\epsilon_s}\frac{W_{pB}}{R}\right)^2+1}. \tag{15}$$

We have found that this equation is within 10% error for

$$\frac{W_p}{R} \leq \frac{3\pi}{8}\left(\frac{S}{R}-1\right), \tag{16}$$

which may be used to derive the NF separation in the array for which the NFs can be regarded as isolated.

For small R, i.e., for sheet-like NFs, we can neglect the unity term under the square root on the RHS of Eq. (12), and use $S-R \approx S$ to obtain

$$W_p \approx \frac{4\epsilon_a V_p}{qN_A}\frac{\tanh\left[\pi S/2W_p\right]}{\pi R} = \frac{8\epsilon_a V_p \tanh\left[\pi S/2W_p\right]}{\pi q N_S}, \tag{17}$$

where the latter form of this equation is useful when NFs are characterized by surface doping $N_S = 2RN_A$ rather than volume doping N_A and thickness $2R$. For small $\pi S/2W_p$, we have $\tanh[\pi S/2W_p] \approx \pi S/2W_p$, and Eq. (17) reduces to the following equation analogous to Eq. (13):

$$W_p \approx \sqrt{\frac{2\epsilon_a V_p S}{qN_A R}} = \sqrt{\frac{4\epsilon_a V_p S}{qN_S}}. \tag{18}$$

This equation can also be obtained from Eq. (13) by neglecting the unity term inside the square root of the ζ expression, and writing $S/R-1 \approx S/R$. The latter form of Eq. (18) matches with the equation derived in Ref. 12. However, the approach of Ref. 12 is more complicated, and involves conformal mapping which cannot yield a model such as our Eq. (12) for a general film thickness. For small R and large S, the NF behaves like an isolated sheet for which, in Eq. (17), $\tanh[\pi S/2W_p] \rightarrow 1$ so that

$$W_p \approx 8\epsilon_a V_p/\pi q N_S. \tag{19}$$

Thus, our approach recovers a result reported in Refs. 15, 20–24 that, in the limiting case of a single sheet-like NF, the junction depletion width variation with potential drop is linear rather than square-root (as in a bulk junction). However, the expression reported in Refs. 20–24 is 21% lower than Eq. (19) derived in our present and previous[15] works.

B. Nanowire array

Application of the solution methodology presented in Section IV to an NW array results in the following implicit equation for W_p (see Appendix A 2)

$$\frac{W_p}{W_{pB}} \approx \sqrt{1+2\frac{\epsilon_a}{\epsilon_s}\frac{T(\pi/2W_p)}{\pi R/2W_p}}, \tag{20}$$

where W_{pB} is given by Eq. (1), and $T(\pi/2W_p)$ by Eq. (A6) with $k_m = k_0 = \pi/2W_p$.

Using Taylor's series expansion of $T(\pi/2W_p)$ around $R/W_p = 0$ and $S/R = 1$, and neglecting the higher order terms, we have

$$\frac{T(\pi/2W_p)}{\pi R/2W_p} \approx \frac{1}{2}\left[\left(\frac{S}{R}\right)^2-1\right] \quad \text{for small} \quad \frac{R}{W_p}, \frac{S}{R}. \tag{21}$$

Substitution of this approximation in Eq. (20) yields the following closed-form equation, analogous to Eq. (13) of the NF array:

$$W_p \approx \zeta W_{pB} \quad \text{where} \quad \zeta = \sqrt{1+\frac{\epsilon_a}{\epsilon_s}\left[\left(\frac{S}{R}\right)^2-1\right]}. \tag{22}$$

We have found that this equation is within 10% error for

$$\frac{W_p}{R} \geq 2.7\left(\frac{S}{R}-1\right)^{1.11}. \tag{23}$$

For large S/R, we have $T(k_0) \approx K_1(\pi R/2W_p)/K_0(\pi R/2W_p)$, where K_0 and K_1 are the modified Bessel functions of second kind, so that Eq. (20) yields

$$\frac{W_p}{W_{pB}} \approx \sqrt{1+2\frac{\epsilon_a}{\epsilon_s}\frac{K_1(\pi R/2W_p)}{K_0(\pi R/2W_p)\pi R/2W_p}}, \tag{24}$$

which can be used for isolated NWs.

For small R, i.e., for thin wires, equation analogous to Eq. (17) can be obtained from Eq. (20). Further, in Eq. (22), we can neglect the unity term inside the square root of the ζ expression, and write $(S/R)^2 - 1 \approx (S/R)^2$ to obtain

$$W_p \approx \sqrt{\frac{2\epsilon_a V_p}{qN_A}\left(\frac{S}{R}\right)^2} = \sqrt{\frac{2\pi\epsilon_a V_p S^2}{qN_L}}, \tag{25}$$

where the latter form of the equation is useful when NWs are characterized by line doping $N_L = \pi R^2 N_A$ rather than volume doping N_A and radius R.

For small R and large S, i.e., for an isolated (single) thin NW, we have (see Appendix A 2)

$$W_p = 1.1R\exp\left(\frac{\epsilon_a}{\epsilon_s}\frac{W_{pB}^2}{R^2}\right) = 1.1R\exp\left(\frac{2\pi\epsilon_a V_p}{qN_L}\right). \tag{26}$$

Thus, the W_p of a single NW junction has an exponential dependence on potential drop and inverse line doping $N_L = N_A \times \pi R^2$. This is in contrast with the square root dependence of the bulk depletion width W_{pB} on potential drop and inverse volume doping N_A. Although Refs. 25 and 26 also derive expressions for depletion width which are exponential like Eq. (26), these expressions yield orders of magnitude higher values and have not been validated against simulations or experiments. The expression derived in Ref. 12 is closer to our Eq. (26). However, Ref. 12 treats the case of a single NW, unlike our present work which treats the more general and realistic case of an array of NWs.

C. Nanotube array

As mentioned in Section III, an NT array is analogous to an NW array with $\epsilon_s = \epsilon_a$, and zero space-charge but non-zero interface charge. Thus, analogous to Eq. (20) of the NW array, we have W_p in an NT array given by (see Appendix A 3)

$$\frac{W_p}{W_{pBT}} \approx \sqrt{1+2\frac{T(\pi/2W_p)}{\pi R/2W_p}}, \tag{27}$$

where W_{pBT} is given by Eq. (A10).

For small R/W_p and S/R, Eq. (27) yields the following closed-form equation, analogous to Eqs. (13) and (22):

$$W_p \approx \zeta W_{pBT} = \sqrt{\frac{\epsilon_a V_p S^2}{qN_S R}} \quad \text{where} \quad \zeta = \frac{S}{R}. \tag{28}$$

Equations for an NT array, which are analogous to Eqs. (24), (25), and (26) of the NW array, can be obtained by replacing ϵ_s by ϵ_a and N_A by $2N_S/R$. Note that, in Eqs. (25) and (26), $N_L = 2\pi R N_S$ for an NT array. It is of interest to note that the values of depletion width in a single NT junction obtained from the approximate expression derived in Ref. 27 are orders of magnitude higher than our results.

D. Model results

Fig. 4(a) shows W_p as a function of R with S as the parameter, and Fig. 4(b) shows W_p as a function of S with R as the parameter. Both figures show that the results of simple closed-form Eq. (13) for NFs and Eq. (22) for NWs match well with the corresponding accurate numerical Eq. (A4) and Eq. (A5) for practical separation S. Moreover, W_p in an NW array can be one order of magnitude higher than that in an NF array, which in turn can be one order of magnitude higher than that in the bulk. Note that, in Fig. 4(b), W_p saturates for large S even though the extent of z over which the normal field E_x in NF and E_r in NW terminates increases with S. This is because the strength of E_x or E_r at large z is too low to cause full depletion. The depletion width model will be validated in Section VII B.

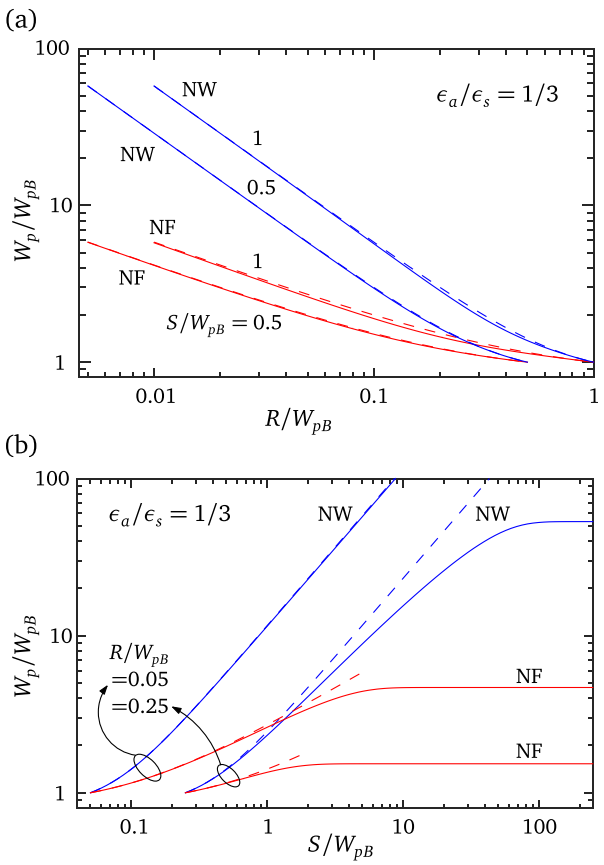

FIG. 4. (a) Depletion width as a function of NF/NW thickness with inter-film/wire separation as the parameter. (b) Depletion width as a function of inter-film/wire separation with NF/NW thickness as the parameter. Solid lines: Eq. (A4) for NF and Eq. (A5) for NW; dashed lines: closed form Eq. (13) for NF and Eq. (22) for NW.

VI. SPACE-CHARGE TAIL AND SCREENING LENGTH

A. Model

As pointed out in Section I, the SCR consists of a partially depleted tail beyond the completely depleted region. A knowledge of this SCR tail width is useful for accurate estimation of the onset of phenomena which depend upon electrostatic interaction between adjacent junctions of the device.[13]

In a bulk junction, the p-side SCR tail width beyond the depletion width W_{pB} is 2–3 times the screening length, also called the Debye length, L_{Dp}. This length is obtained from the potential distribution $\varphi \sim \exp(-z/L_{Dp})$, derived under the linear screening condition,[16] i.e., the space-charge density is proportional to the potential.[28] Similar treatment for junctions in NF/NW/NT arrays given in Appendix B leads to the following equation for the potential in the p-side SCR tail, i.e., for φ at large z:

$$\frac{\varphi(R^+,z)}{V_p} = 1 - \frac{2}{\pi}\int_0^\infty \frac{\sin(\lambda z)/\lambda \quad d\lambda}{1+L_{Ap}^2\lambda^2}, \tag{29}$$

where

$$L_{Ap} = \begin{cases} \zeta L_{Dp} & \text{for NF and NW arrays}, \\ \zeta L_{DpT} & \text{for NT arrays}. \end{cases} \tag{30}$$

Here, ζ is given by Eq. (13) for NF arrays, Eq. (22) for NW arrays, and Eq. (28) for NT arrays, and L_{DpT} is given by Eq. (B9). Writing the unity term on the RHS of Eq. (29) as $\int_0^\infty [2\sin(\lambda z)/\pi\lambda]d\lambda$, and identifying the resulting expression to be the inverse Fourier Transform representation of an exponential function, we have from Eq. (29)

$$\frac{\varphi(R^+,z)}{V_p} = \frac{2}{\pi}\int_0^\infty \frac{L_{Ap}^2\lambda\sin(\lambda z)\,d\lambda}{1+L_{Ap}^2\lambda^2} = \exp\left(-z/L_{Ap}\right). \tag{31}$$

This equation is similar to the potential distribution $\varphi \sim \exp(-z/L_{Dp})$ in a bulk semiconductor under linear screening.[16] Thus, we conclude that the SCR tail in arrays of NF/NW/NT junctions behaves similar to that in a bulk junction with an increased screening length L_{Ap}, and that the SCR tail width is 2–3 times L_{Ap}. This bulk-like behavior of SCR tail in NF/NW/NT arrays is due to the mutual screening of NFs/NWs/NTs at large z.

B. Model validation

We consider Schottky junctions for validation. However, the results hold good for p-n junctions as well. Fig. 5 shows the simulated equilibrium space-charge distributions in a variety of Schottky junctions in bulk and NF/NW/NT arrays. The simulations of NF and NW arrays are carried out in Sentaurus TCAD,[18] and those of NT array are carried out in Matlab employing the methodology described in Ref. 14. The inset of Fig. 5 brings out the significance of the screening length L_{Ap} by showing that the space-charge density curves of Fig. 5 merge when plotted in a normalized form, wherein the space-charge in bulk, NF, and NW are normalized to qN_A, the surface-charge in NT is normalized to qN_S, and the distance z is normalized to L_{Ap}. This normalized plot also serves as a validation of our screening length model.

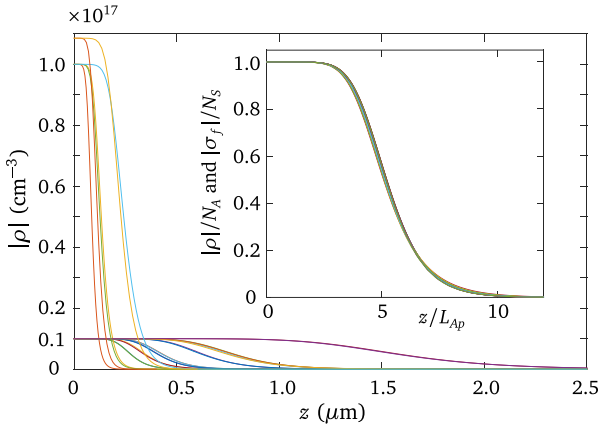

FIG. 5. Simulated equilibrium space-charge distributions of a Schottky junction realized in bulk silicon, and in arrays of silicon NFs/NWs and carbon NTs in SiO_2/HfO_2 ambient. Simulations of NF/NW arrays use some combinations of the following parameters: $\epsilon_s = 11.7\epsilon_0$; $\epsilon_a = 3.9\epsilon_0, 18\epsilon_0$; $R = 10$, 20 nm; $S/R = 3, 6$; $N_A = 10^{16}, 10^{17}\,\text{cm}^{-3}$; and $V_p = 0.4$ V. Simulations of carbon NT arrays use $\epsilon_a = 3.9\epsilon_0$; $R = 0.7$ nm; $S/R = 3, 6$; $N_S = 3.8\times10^9\,\text{cm}^{-2}$ (equivalent to $N_A = 2N_S/R \approx 1.1\times10^{17}\,\text{cm}^{-3}$); and $V_p = 0.4$ V. The inset shows that all these distributions merge into a single curve when plotted in a normalized form.

VII. EFFECTIVE MEDIUM THEORY (EMT)

A. Physical interpretation of depletion width and screening length formulas

Consider the closed-form depletion width models $W_p = \zeta W_{pB}$ for NF/NW arrays and $W_p = \zeta W_{pBT}$ for NT arrays, and the screening length models $L_{Ap} = \zeta L_{Dp}$ for NF/NW arrays and $L_{Ap} = \zeta L_{DpT}$ for NT arrays. Here ζ is given by Eq. (13) for NF arrays, Eq. (22) for NW arrays, and Eq. (28) for NT arrays. Using the W_{pB} and L_{Dp} expressions of Eq. (1) in the above equations, the depletion width W_p and the screening length L_{Ap} can be written in the form of Eq. (2), where ϵ_{emt} and N_{Aemt} are given by

$$\epsilon_{emt} = \frac{\epsilon_s 2RU + \epsilon_a(2S-2R)U}{2SU} \quad \text{and} \quad N_{Aemt} = \frac{N_A 2R}{2S} \tag{32}$$

for an NF array of side width U in y-direction,

$$\epsilon_{emt} = \frac{\epsilon_s \pi R^2 + \epsilon_a(\pi S^2 - \pi R^2)}{\pi S^2} \quad \text{and} \quad N_{Aemt} = \frac{N_A \pi R^2}{\pi S^2} \tag{33}$$

for an NW array, and

$$\epsilon_{emt} = \epsilon_a \quad \text{and} \quad N_{Aemt} = \frac{N_S 2\pi R}{\pi S^2} \tag{34}$$

for an NT array.

The above Eqs. (32)–(34) can be unified together by writing ϵ_{emt} and N_{Aemt} as in Eq. (3). Note that ϵ_{emt} and N_{Aemt} capture the geometrical parameters of the array, i.e.,

NF/NW/NT thickness and inter-NF/NW/NT separation, in the form of the cross-sectional areas A_s of the semiconductor and A_a of the ambient dielectric, where

$$\begin{aligned} A_s &= 2RU\,, \quad A_a = 2SU \quad \text{for} \quad \text{NF} \\ A_s &= \pi R^2\,, \quad A_a = \pi(S^2 - R^2) \quad \text{for} \quad \text{NW/NT}. \end{aligned} \tag{35}$$

Thus, we have arrived at an Effective Medium Theory for the space-charge region electrostatics of arrays of nanoscale junctions, as per which, the depletion width and the screening length characterizing the SCR tail in the array correspond to those in a bulk junction with an effective semiconductor medium, whose permittivity and doping are their weighted averages over the cross-sectional areas of the semiconductor and dielectric. Here, the doping has the effective value given by Eq. (11) if σ_f is non-zero. Although derived considering square lattice of NWs/NTs having circular cross-section, the theory is generally applicable to other shapes of NW/NT cross-sections and lattice, i.e., for given values of A_s and A_a, the depletion width and screening length are independent of the shapes of the NW/NT cross-section and lattice; the NW/NT cross-section could be circular, square, triangular, hexagonal, etc., and the lattice could be square, honeycomb, triangular, etc. This is confirmed in Section VII B below.

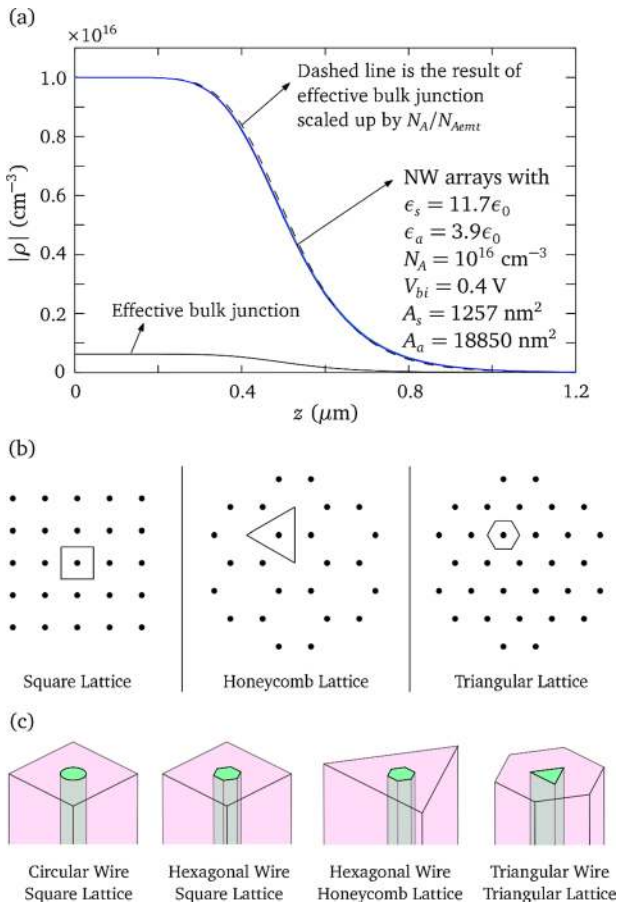

FIG. 6. (a) 3D simulations of equilibrium space-charge distributions of Schottky junctions realized in various arrays of silicon NWs in SiO_2 ambient. In all arrays, the NWs have same cross-sectional area A_s, and the ambient dielectric has the same cross-sectional area A_a. The arrays employed can be denoted as CS, SS, HS, HT, HH, TT, and TH; here, the first letter denotes the NW cross-section—circular (C), square (S), hexagonal (H) or triangular (T); the second letter denotes the lattice-square (S), honeycomb (H), or triangular (T), whose unit cell has the ambient cross—section shown in (b). For illustration, (c) shows the 3D view of unit cells of CS, HS, HH, and TT arrays.

B. EMT validation

We validate our theory considering arrays of NW junctions. Similar results hold good for NF and NT arrays.

Fig. 6 shows the three-dimensional simulations of space-charge distributions in various arrays of NW Schottky junctions. It is seen that, for given values of A_s and A_a, not only the depletion width and screening length, but the entire space-charge distribution is independent of the shapes of the NW cross-section and lattice. This has an important corollary: the space-charge distribution in an NW/NT array of an arbitrary 3D configuration can be predicted from a 2D simulation of a unit cell having circular cross-sections of NW/NT and ambient. Also included in Fig. 6 is the space-charge distribution of a bulk Schottky junction in an effective semiconductor medium having a permittivity ϵ_{emt} and doping N_{Aemt}, together with its scaled version wherein the space-charge is scaled up by N_A/N_{Aemt}; the potential drops across the bulk and NW junctions are kept same. It is seen that the scaled bulk version overlaps with the NW space-charge distributions. These results support our Effective Medium Theory. This theory based on Eqs. (13), (22), and (28) is valid over the range specified by Eq. (14) for NF arrays and Eq. (23) for NW/NT arrays, which cover all practical arrays.

As a further confirmation, Fig. 7 establishes that the TCAD simulated small-signal reverse bias Capacitance-Voltage (C-V) characteristics of Schottky and p-n junctions in NW arrays are predicted by the following C-V model of a bulk junction with parameters of the effective medium theory. The junction capacitance over a unit cell area $A_s + A_a$ is

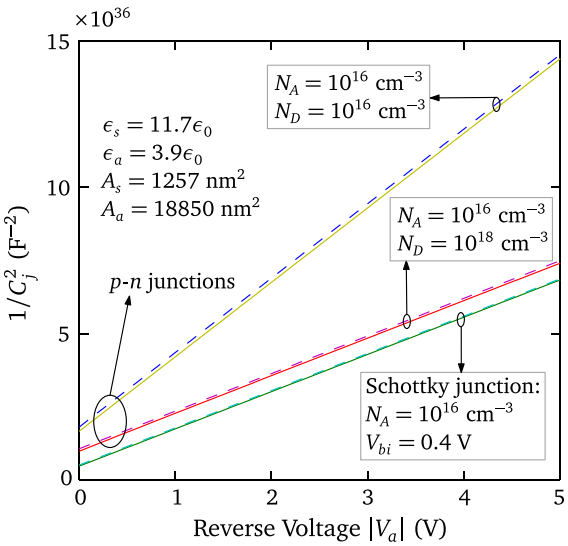

FIG. 7. The small-signal reverse bias capacitance-voltage characteristics of Schottky and p-n junctions realized in arrays of silicon NWs in SiO_2 ambient. Solid lines are numerical simulations of actual structures, and dashed lines are analytical calculations as per Effective Medium Theory.

$$C_j = \epsilon_{emt}(A_s + A_a)/W\,, \tag{36}$$

where W is the total depletion width given by

$$W = \sqrt{\frac{2\epsilon_{emt}(V_{bi} - V_a)}{qN_{Aemt}}} \tag{37}$$

for p-type Schottky junctions, and

$$W = W_p + W_n = \sqrt{\frac{2\epsilon_{emt}(V_{bi} - V_a)}{q}\left(\frac{1}{N_{Aemt}} + \frac{1}{N_{Demt}}\right)} \tag{38}$$

for p-n junctions. The small discrepancy between the simulated and modeled capacitances vanishes if we include the potential drop of $\sim V_t$ across the space-charge tails beyond the depletion edges in the W expressions and write the voltages as $V_{bi} - V_a - V_t$ for Schottky and $V_{bi} - V_a - 2V_t$ for p-n junctions.[17] The significance of this EMT theory is that the doping, built-in potential, and NF/NW/NT length of junctions in NF/NW/NT arrays can be determined from the junction C-V behavior, as in the case of bulk junctions. The slope and voltage intercept of the linear $1/C_j^2$ versus V_a curve yield the doping and built-in voltage, while saturation value of the capacitance yields the NF/NW/NT length.[29] In the presence of σ_f, the extracted doping is the effective value given by Eq. (11), from which σ_f can be obtained if the volume doping is known.

C. Effect of process variations

In the derivation so far, we have assumed the parameters R, S, N_A, and the junction position to be the same for all NFs/NWs/NTs of the array. In this case, A_s and A_a in Eq. (3) correspond to a unit cell of the array, and are given by Eq. (35). However, in practice, R, S, N_A, and the junction position may vary randomly with location in the array due to process variations. In this case, in Eq. (3), we should regard A_s and A_a as the total semiconductor and dielectric areas of the array, $(A_s + A_a)$ as the device area, N_A as the average doping, and the resulting W_p, L_{Ap} in Eq. (2) as the average values. For instance, consider an NW array, wherein the number of wires is n, and the (mean, standard deviation) pair of the wire radii is (μ_R, σ_R), of the wire separations is (μ_S, σ_S), and of the wire dopings is (μ_N, σ_N). In this case, we take $A_s = n\pi(\mu_R^2 + \sigma_R^2), A_a = n\pi[(\mu_S^2 + \sigma_S^2) - (\mu_R^2 + \sigma_R^2)]$, and $N_A = \mu_N$ in Eq. (3) to obtain average values of W_p and L_{Ap} from Eq. (2). Usually, NW arrays are grown or etched using lithographic patterning; in grown wires, junctions are formed by a combination of *in-situ* doping during growth followed by ion-implantation or by *in-situ* doping alone; in etched wires, the junction exists in the starting epitaxial wafer which is etched. Process variations are small in NW junctions fabricated in this manner. However, in junction arrays fabricated by unpatterned NW growth, the process variations can become large enough to make the variation in junction position comparable with the average W_p estimated using Eq. (2). This renders the EMT theory inaccurate. Similar discussion applies to NF/NT arrays as well.

VIII. BUILT-IN VOLTAGE INCLUDING QUANTUM CONFINEMENT

Estimation of W in an array as per Eqs. (37) and (38) requires the knowledge of V_{bi}. In ultra-thin films/wires, the energy levels in the conduction and valence bands are quantized, so that, for a given carrier concentration, the fermi-level moves towards or even into the conduction/valence band as film/wire thickness decreases. This increases V_{bi}, which is the difference in fermi-levels on either side of the junction. Eq. (35) of Ref. 15 gives an expression for this increased V_{bi} in ultra-thin NF p-n junctions. We can extend this approach to other structures as follows.

For a thin NW, which can be regarded as an infinitely deep two-dimensional potential well, the solution of the Schrodinger equation yields the following subband density of states[30]

$$\rho_{\mathrm{DOS}}(E) = \frac{1}{\pi\hbar}\sqrt{\frac{2m^*}{(E - E_{sb})}}, \tag{39}$$

where m^* denotes the electron or hole effective mass, and E_{sb} the subband minima. For an NW of circular cross-section, the subband minimas $E_{sb} = E_{ln}$ are given by[30]

$$\left.\begin{matrix} E_{ln} - E_C \\ E_V - E_{ln} \end{matrix}\right\} = \frac{\hbar^2 j_{ln}^2}{2m^* R^2}\,, \tag{40}$$

where E_C and E_V are the conduction and valence band edges, and j_{ln} is the nth zero of the Bessel function of order l of the first kind $J_l(\cdot)$. In Eqs. (39) and (40), we use an average m^* for all three directions. However, our results apply even when m^* is different in different directions. For nondegenerate doping, only the first subband ($l = n = 1$ and $j_{ln} = 2.405$) is filled, and the hole concentration per unit wire length is

$$p_l = \sqrt{\frac{2m_p^* q V_t}{\pi\hbar^2}}\exp\left(\frac{E_F - E_{11}}{qV_t}\right). \tag{41}$$

We obtain the p-side work function as

$$\phi_{sp} = \chi + (E_C - E_V) + (E_V - E_{11}) + (E_{11} - E_F)\,, \tag{42}$$

where χ is the electron affinity, $E_C - E_V = E_g$ is the semiclassical energy gap, and the remaining terms are given by Eqs. (40) and (41). Then we obtain V_{bi} as $|\phi_m - \phi_{sp}|$ for Schottky junctions, where ϕ_m is the metal work function, and as $|\phi_{sn} - \phi_{sp}|$ for p-n junctions. Here, ϕ_{sn} is the n-side work function obtained from the electron concentration per unit wire length n_l in the same way as ϕ_{sp} is obtained from p_l using Eqs. (40), (41) and (42).

Reference 15 showed that V_{bi} of NF p-n junctions should be estimated including quantum confinement for NFs thinner than 5 nm. Similar calculations performed as earlier show that this thickness limit for NWs is higher (= 10 nm) because of additional degree of confinement. Indeed, for an NW p-n junction with $2R = 10$ nm and $N_A = N_D = 2 \times 10^{17}\,\mathrm{cm}^{-3}$, V_{bi} including quantum confinement is 1.0 V, which is just 13% higher than the classical value of 0.87 V

obtained using $V_{bi} = V_t \log(N_A N_D / n_i^2)$. On the other hand, for $2R = 2$ nm and $N_A = N_D = 5 \times 10^{18}\,\mathrm{cm}^{-3}$, V_{bi} including quantum confinement is 1.8 V, which is 44% higher than the classical value of 1.0 V. In these calculations, we use $m^* = 0.5m_0$ for both electron and hole, $E_g = 1.12$ eV, and $n_i = 10^{10}\,\mathrm{cm}^{-3}$.

We now illustrate that, for a given NW cross-sectional area A_s, V_{bi} is approximately independent of the shape of the NW cross-section. Consider NWs of square cross-section with side $a = \sqrt{A_s}$, for which the subband minimas $E_{sb} = E_{ij}$ are given by[30]

$$\left.\begin{matrix} E_{ij} - E_C \\ E_V - E_{ij} \end{matrix}\right\} = \frac{\hbar^2 \pi^2 \left(i^2 + j^2\right)}{2m^* a^2} \quad i,j = 1,2,3,\ldots \tag{43}$$

For $m^* = 0.5m_0$ and $A_s = 12.57\,\mathrm{nm}^2$, we have $R = 2$ nm and $E_{11} - E_C = 0.11$ eV for circular NWs, and $a = 3.54$ nm and $E_{11} - E_C = 0.12$ eV for square NWs. The difference of 10 meV for the two NWs is negligible when compared with V_{bi} of 0.4 V to 0.8 V. Thus, the increased V_{bi} for NWs of any cross-sectional shape can be obtained from circular or square NWs of same A_s, i.e., the NW cross-sectional shape is immaterial, which is consistent with our EMT theory.

Finally, the doping level used to determine the carrier concentration p_l or n_l should account for interface charge as per Eq. (11) and partial impurity ionization. As we move away from the junction, the difference between the fermi and impurity levels, which represents the extent of impurity ionization, decreases and finally saturates. Therefore, N_A to be used in W_p can be different from that used in L_{Ap}, where saturated N_A value can be used. When volume doping is zero, the effective doping is due to interface charge alone, and is the same in both W_p and L_{Ap} equations.

IX. CONCLUSION

We derived an Effective Medium Theory for the space-charge region electrostatics of arrays of NF/NW/NT junctions, and validated it by comparison with numerical simulations. The theory shows that the depletion width and the screening length characterizing the SCR tail in the array correspond to those in a bulk junction with an effective semiconductor medium, whose permittivity and doping are their weighted averages over the cross-sectional areas of the semiconductor and dielectric. For given cross-sectional areas of semiconductor and dielectric, the space-charge distribution, depletion width, and screening length are independent of the shapes of the semiconductor cross-section and the lattice. Consequently, the space-charge distribution in an NW/NT array of an arbitrary 3D configuration can be predicted from a 2D simulation of a unit cell having circular cross-sections of NW/NT and dielectric. The EMT theory shows that the reverse bias $1/C^2$–V behavior of junctions in NF/NW/NT arrays is linear, and can be used to extract the built-in potential, effective doping, which includes the semiconductor-dielectric interface charge, and NF/NW/NT length. The theory is useful for the experimentalist and yields simple formulas for nano-device design. While using these formulas for ultra-thin structures, the built-in voltage needs to be estimated using quantum effects. The formulas predict that, in the limiting case of a single sheet-like NF, the junction depletion width variation with potential drop is linear rather than square-root (as in a bulk junction). Moreover, in arrays of symmetric silicon p-n junctions in oxide dielectric where NF/NW thickness and separation are 5% and 100% of the bulk depletion width, respectively, the junction depletion width and the screening length are scaled up from their bulk values by the same factor of ~2 for NF and ~10 for NW array.

APPENDIX A: DERIVATION OF JUNCTION DEPLETION WIDTH

1. Nanofilm array

Refer to Fig. 3(c) and the solution methodology in Section IV. For the boundary conditions $\partial\varphi/\partial x = 0$ at $x = S$, $\varphi = V_p$ at $z = 0$, and $\partial\varphi/\partial z = 0$ at $z = W_p$, the general solution of Laplace's equation in the dielectric is

$$\varphi(x,z) = V_p - \sum_{m=0}^{\infty} B_m \frac{\sin(k_m z)\cosh[k_m(S-x)]}{\cosh[k_m(S-R)]}, \tag{A1}$$

where $k_m = (2m+1)\pi/2W_p$. The $\cosh[k_m(S-R)]$ term in the denominator of the summation is included for mathematical convenience as will be evident shortly from the expression for B_m. From the complete depletion approximation, we have

$$\rho(x,z) = \begin{cases} -qN_A & \text{for} \quad 0 < z \le W_p, \\ 0 & \text{for} \quad z > W_p. \end{cases} \tag{A2}$$

Substitution of $\rho = -qN_A$ from this equation, $\sigma_f = 0$, and $\partial\varphi(R^+,z)/\partial x$ and $\partial^2\varphi(R^+,z)/\partial z^2$ obtained from Eq. (A1) into Eq. (8) yields an equation for B_m, which can be solved using Fourier series techniques to get

$$B_m = \frac{16}{\pi^3}\frac{qN_A W_p^2}{\epsilon_s}\frac{1/(2m+1)^3}{\left[1 + \frac{\epsilon_a}{\epsilon_s}\frac{\tanh[k_m(S-R)]}{k_m R}\right]}. \tag{A3}$$

From the constant φ approximation and the discussion on the $z = W_p$ boundary condition in the last paragraph of Section III, we have $\varphi(R,W_p) \approx \varphi(0,W_p) = 0$. Setting $\varphi(R,W_p) \approx 0$ in Eq. (A1), we get $V_p = \sum_0^\infty (-1)^m B_m$. Substituting Eq. (A3) for B_m in this equation, and rearranging, we obtain the following implicit equation for W_p, which can be solved iteratively

$$\frac{W_p}{W_{pB}} = \sqrt{\alpha}\left[\sum_{m=0}^{\infty}\frac{(-1)^m/(2m+1)^3}{1 + \frac{\epsilon_a}{\epsilon_s}\frac{\tanh[k_m(S-R)]}{k_m R}}\right]^{-\frac{1}{2}}, \tag{A4}$$

where $\alpha = \sum_0^\infty (-1)^m/(2m+1)^3 = \pi^3/32 \approx 0.97$ and W_{pB} is given by Eq. (1). A quick validation of Eq. (A4) is that, for $\epsilon_a \ll \epsilon_s$ (weak ambient field) or large R (thick NF) or $S \to R$ (closely packed NFs), $W_p \to W_{pB}$, as it should. In Eq. (A4),

$m=0$ term dominates the summation. Using the $m=0$ term alone, this summation can be approximated to $\alpha[1+\epsilon_a \tanh[k_0(S-R)]/\epsilon_s k_0 R]^{-1}$, where $k_0=\pi/2W_p$, yielding Eq. (12).

2. Nanowire array

Applying the above procedure to an NW array yields[14]

$$\frac{W_p}{W_{pB}}=\sqrt{\alpha}\left[\sum_{m=0}^{\infty}\frac{(-1)^m/(2m+1)^3}{1+2\frac{\epsilon_a}{\epsilon_s}\frac{T(k_m)}{k_mR}}\right]^{-\frac{1}{2}}, \tag{A5}$$

where

$$T(k_m)=\frac{I_1(k_mS)K_1(k_mR)-I_1(k_mR)K_1(k_mS)}{I_1(k_mS)K_0(k_mR)+I_0(k_mR)K_1(k_mS)}, \tag{A6}$$

and I_0, I_1 and K_0, K_1 are the modified Bessel functions. As done in the case of NF array, by approximating Eq. (A5) with the $m=0$ term alone, we obtain Eq. (20).

For a single NW, i.e., for $S\to\infty$, we have $R\ll W_p$ so that $T(k_m)\to K_1(k_mR)/K_0(k_mR)\approx[k_mR(\log(2/k_mR)-\gamma)]^{-1}$, where $\gamma\approx0.58$ is the Euler's constant. Neglecting the unity term in the denominator of the summation in Eq. (A5) for small $R\ll W_p$, and using the above approximate $T(k_m)$ in Eq. (A5), we have

$$\sum_{m=0}^{\infty}\frac{(-1)^m}{(2m+1)}\log\left[\frac{4W_p}{(2m+1)\pi Re^{\gamma}}\right]=\frac{8\alpha}{\pi^2}\frac{\epsilon_a}{\epsilon_s}\left(\frac{W_{pB}}{R}\right)^2. \tag{A7}$$

Using the identities $a\log b=\log b^a$ and $\log a+\log b=\log ab$ in the above summation, we get

$$\frac{\left(\frac{4W_p}{\pi Re^{\gamma}}\right)^{\sum_{m=0}^{\infty}\frac{(-1)^m}{(2m+1)}}}{\prod_{m=0}^{\infty}(2m+1)^{\frac{(-1)^m}{(2m+1)}}}=\exp\left[\frac{8\alpha}{\pi^2}\frac{\epsilon_a}{\epsilon_s}\left(\frac{W_{pB}}{R}\right)^2\right]. \tag{A8}$$

Using $\sum_0^{\infty}(-1)^m/(2m+1)=\pi/4$, $\prod_0^{\infty}(2m+1)^{(-1)^m/(2m+1)}=0.825$, and $\alpha=\sum_0^{\infty}(-1)^m/(2m+1)^3=\pi^3/32$, we obtain Eq. (26) for W_p in a single NW.

3. Nanotube array

We obtain W_p in an NT array from that in an NW array as follows. In Eq. (10), we let $\rho+2\sigma_f/R=\rho_{eff}$, where ρ_{eff} is the effective space-charge density. While $\rho_{eff}=\rho=-qN_A$ for an NW array having $\sigma_f=0$, we have $\rho_{eff}=0+2\sigma_f/R=-2qN_S/R$ for an NT array, where N_S is the surface doping in the NT. Thus, by comparing the ρ_{eff} expressions of NW and NT arrays, we obtain W_p in an NT array from Eq. (A5) of an NW array by replacing ϵ_s by ϵ_a and N_A by $2N_S/R$, i.e.,

$$\frac{W_p}{W_{pBT}}=\sqrt{\alpha}\left[\sum_{m=0}^{\infty}\frac{(-1)^m/(2m+1)^3}{1+2\frac{T(k_m)}{k_mR}}\right]^{-\frac{1}{2}}, \tag{A9}$$

where

$$W_{pBT}=\sqrt{\frac{\epsilon_aV_pR}{qN_S}}=\sqrt{\frac{2\epsilon_aV_p}{q(N_S\times2\pi R/\pi R^2)}} \tag{A10}$$

is the bulk depletion width expression W_{pB} in Eq. (1) with N_A replaced by $2N_S/R$. The expression $2N_S/R$ can be interpreted as the volume doping obtained by distributing the NT surface doping N_S uniformly over the NT cross-sectional area, i.e., $N_A=N_S\times2\pi R/\pi R^2$. Note that, W_{pBT} is the value of W_p for $S\to R$, and was denoted as $W_{S\to R}$ in Ref. 14. As done in the case of NF and NW arrays, by approximating Eq. (A9) with the $m=0$ term alone, we obtain Eq. (27).

APPENDIX B: DERIVATION OF SPACE-CHARGE TAIL AND SCREENING LENGTH

1. Nanofilm array

Refer to Fig. 3(c). The boundary conditions are $\partial\varphi/\partial x=0$ at $x=S$, $\varphi=V_p$ at $z=0$, and $\varphi\to0$ for $z\to\infty$. The condition $\varphi\to0$ for $z\to\infty$ differs from the condition $\partial\varphi/\partial z=0$ at $z=W_p$ employed in W_p derivation, since we need φ over the space-charge tail beyond W_p. For these boundary conditions, the general solution of the Laplace's equation in the dielectric is

$$\varphi(x,z)=V_p-\int_0^{\infty}A(\lambda)\sin(\lambda z)\frac{\cosh[\lambda(S-x)]}{\cosh[\lambda(S-R)]}d\lambda. \tag{B1}$$

We can obtain φ for all z if we know $A(\lambda)$ for all λ, which in turn can be obtained if we know $\rho(z)$ for all z. For $z<W_p$, we have $\rho(z)\approx-qN_A$. For large z, i.e., in the SCR tail, we can approximate $\rho(z)$ as follows. Since φ falls below V_t beyond W_p and is $\ll V_t$ in the SCR tail, linear screening prevails in the tail region, i.e., ρ is proportional to φ as per $\rho=q^2(\partial p/\partial E_F)\varphi$, where p is the hole density and E_F is the Fermi-level.[28] For non-degenerate doping, p is given by the Boltzmann distribution, and so, $\partial p/\partial E_F=-p/qV_t=-N_A/qV_t$. Substituting this in $\rho=q^2(\partial p/\partial E_F)\varphi$ and using Eq. (1), we have

$$\rho=q^2(\partial p/\partial E_F)\varphi=-qN_A\varphi/V_t=-\epsilon_s\varphi/L_{Dp}^2. \tag{B2}$$

Since the variation of ρ between $z=W_p$ and the SCR tail is not known, we cannot obtain $A(\lambda)$ for all values of λ, and hence, φ for all values of z. However, we can obtain φ for large z, i.e., in the SCR tail which is of our interest, from an approximate expression of $A(\lambda)$ for small λ. This is due to the fact that only small values of λ contribute to the integral in Eq. (B1), since z is large for the SCR tail and $\sin(\lambda z)$ is an oscillatory function. Substitution of $\rho=-\epsilon_s\varphi/L_{Dp}^2$ (from Eq. (B2)), $\sigma_f=0$, and $\partial\varphi(R^+,z)/\partial x$ and $\partial^2\varphi(R^+,z)/\partial z^2$ obtained from Eq. (B1) into Eq. (8) results in the following equation valid for large z:

$$\int_0^{\infty}\frac{1+\frac{\epsilon_aL_{Dp}^2}{\epsilon_sR}\lambda\tanh[\lambda(S-R)]+L_{Dp}^2\lambda^2}{V_p}A(\lambda)\sin(\lambda z)d\lambda=1. \tag{B3}$$

Writing the unity term on the RHS of the above equation as $\int_0^\infty [2\sin(\lambda z)/\pi\lambda]d\lambda$, and then comparing the LHS and RHS, we obtain $A(\lambda)$ for small λ as

$$A(\lambda) = \frac{2V_p/\pi\lambda}{1 + \frac{\epsilon_a L_{Dp}^2}{\epsilon_s R}\lambda\tanh[\lambda(S-R)] + L_{Dp}^2\lambda^2}. \quad \text{(B4)}$$

From Eqs. (B1) and (B4), we get φ for large z as

$$\frac{\varphi(R^+,z)}{V_p} = 1 - \frac{2}{\pi}\int_0^\infty \frac{\sin(\lambda z)/\lambda \quad d\lambda}{1 + \frac{\epsilon_a L_{Dp}^2}{\epsilon_s R}\lambda\tanh[\lambda(S-R)] + L_{Dp}^2\lambda^2}. \quad \text{(B5)}$$

Considering that only small λ contributes to the integral in the above equation, we have $\tanh[\lambda(S-R)] \approx \lambda(S-R)$, so that Eq. (B5) yields Eq. (29).

2. Nanowire array

For the boundary conditions shown in Fig. 3(c), the general solution of Laplace's equation in the dielectric is

$$\varphi(r,z) = V_p - \int_0^\infty A(\lambda)\sin(\lambda z) \times \left\{\frac{I_1(\lambda S)K_0(\lambda r) + I_0(\lambda r)K_1(\lambda S)}{I_1(\lambda S)K_0(\lambda R) + I_0(\lambda R)K_1(\lambda S)}\right\} d\lambda. \quad \text{(B6)}$$

Following the same procedure as above, we obtain φ for large z, i.e., in the SCR tail

$$\frac{\varphi(R^+,z)}{V_p} = 1 - \frac{2}{\pi}\int_0^\infty \frac{\sin(\lambda z)/\lambda}{1 + 2\frac{\epsilon_a}{\epsilon_s}\frac{L_{Dp}^2}{R}\lambda T(\lambda) + L_{Dp}^2\lambda^2} d\lambda, \quad \text{(B7)}$$

where $T(\lambda)$ is obtained from Eq. (A6) by replacing k_m by λ. Considering that only small λ contributes to the integral in the above equation, we have $T(\lambda)/\lambda R \approx (1/2)[(S/R)^2 - 1]$, like in Eq. (21), so that Eq. (B7) yields Eq. (29).

3. Nanotube array

Note that Eq. (B2) is not applicable for an NT array because, in an NT array, we have zero volume charge but non-zero surface charge σ_f. When the NT surface doping N_S is non-degenerate, the surface hole concentration $p_s \propto \exp(-E_F/kT)$, and therefore, $\partial p_s/\partial E_F = -N_S/qV_t$. This can be verified, for example, from the analytical expression of the carrier concentration in a carbon nanotube under non-degenerate doping derived in Ref. 31. Thus, we have for an NT array

$$\sigma_f = q^2(\partial p_s/\partial E_F)\varphi = -qN_S\varphi/V_t. \quad \text{(B8)}$$

This equation can also be derived from Eq. (B2) by replacing ρ by $2\sigma_f/R$ $(= 2\pi R\sigma_f/\pi R^2)$ and N_A by $2N_S/R$.

Following the derivation similar to that of NW array, we obtain Eq. (B7) with L_{Dp} replaced by

$$L_{DpT} = \sqrt{\epsilon_a V_t R/2qN_S}, \quad \text{(B9)}$$

which can be obtained from $L_{Dp} = \sqrt{\epsilon_s V_t/qN_A}$ by replacing ϵ_s by ϵ_a and N_A by $2N_S/R$, in much the same way as Eq. (A10) for W_{pBT} is obtained from W_{pB}. Further analysis as in the case of NW array yields Eq. (29).

[1]M. Yao, N. Huang, S. Cong, C.-Y. Chi, M. A. Seyedi, Y.-T. Lin, Y. Cao, M. L. Povinelli, P. D. Dapkus, and C. Zhou, Nano Lett. **14**, 3293 (2014).
[2]P. Zhang, P. Liu, S. Siontas, A. Zaslavsky, D. Pacifici, J.-Y. Ha, S. Krylyuk, and A. Davydov, J. Appl. Phys. **117**, 125104 (2015).
[3]E. Lai, W. Kim, and P. Yang, Nano Res. **1**, 123 (2008).
[4]S. Hersee, M. Fairchild, A. K. Rishinaramangalam, M. S. Ferdous, L. Zhang, P. Varangis, B. S. Swartzentruber *et al.*, Electron. Lett. **45**, 75 (2009).
[5]C. Pan, L. Dong, G. Zhu, S. Niu, R. Yu, Q. Yang, Y. Liu, and Z. L. Wang, Nat. Photonics **7**, 752 (2013).
[6]H. Guo, Z. Lin, Z. Feng, L. Lin, and J. Zhou, J. Phys. Chem. C **113**, 12546 (2009).
[7]C.-L. Hsu, S.-J. Chang, Y.-R. Lin, P.-C. Li, T.-S. Lin, S.-Y. Tsai, T.-H. Lu, and I.-C. Chen, Chem. Phys. Lett. **416**, 75 (2005).
[8]W. Wei, X.-Y. Bao, C. Soci, Y. Ding, Z.-L. Wang, and D. Wang, Nano Lett. **9**, 2926 (2009).
[9]Q. Zeng, S. Wang, L. Yang, Z. Wang, T. Pei, Z. Zhang, L.-M. Peng, W. Zhou, J. Liu, W. Zhou *et al.*, Opt. Mater. Express **2**, 839 (2012).
[10]P.-H. Su and Y. Li, IEEE Trans. Electron Devices **62**, 1663 (2015).
[11]Z. Liu, L. Song, S. Zhao, J. Huang, L. Ma, J. Zhang, J. Lou, and P. M. Ajayan, Nano Lett. **11**, 2032 (2011).
[12]A. Achoyan, S. Petrosyan, W. Craig, H. Ruda, and A. Shik, J. Appl. Phys. **101**, 104308 (2007).
[13]S. Karmalkar, IEEE Trans. Electron Devices **45**, 2187 (1998).
[14]V. K. Gurugubelli and S. Karmalkar, Appl. Phys. Lett. **104**, 203502 (2014).
[15]V. K. Gurugubelli and S. Karmalkar, J. Appl. Phys. **118**, 034503 (2015).
[16]M. Shur, *Physics of Semiconductor Devices* (Prentice-Hall, Inc., 1990).
[17]S. M. Sze and K. K. Ng, *Physics of Semiconductor Devices* (John Wiley & Sons, 2006).
[18]*Sentaurus Device User Guide*, Synopsys (2013).
[19]N. Averkiev and A. Shik, Phys. Rev. B **59**, 3250 (1999).
[20]S. Petrosyan and A. Y. Shik, Sov. Phys. JETP **69**, 1261 (1989); [Zh. Eksp. Teor. Fiz. **96**, 2229–2239 (1989)]; available at jetp.ac.ru/cgi-bin/dn/e_069_06_1261.pdf.
[21]B. Gelmont, M. Shur, and C. Moglesture, IEEE Trans. Electron Devices **39**, 1216 (1992).
[22]A. S. Achoyan, A. Yesayan, E. Kazaryan, and S. Petrosyan, Semiconductors **36**, 903 (2002).
[23]C. Wiemann, M. Versen, and A. Wieck, J. Vac. Sci. Technol. B **16**, 2567 (1998).
[24]D. Reuter, C. Werner, A. Wieck, and S. Petrosyan, Appl. Phys. Lett. **86**, 162110 (2005).
[25]H. Ruda and A. Shik, Appl. Phys. Lett. **85**, 1030 (2004).
[26]F. Léonard, A. A. Talin, B. Swartzentruber, and S. Picraux, Phys. Rev. Lett. **102**, 106805 (2009).
[27]F. Léonard and J. Tersoff, Phys. Rev. Lett. **83**, 5174 (1999).
[28]N. W. Ashcroft and N. D. Mermin, *Solid State Physics* (Brooks Cole, 1976).
[29]M. S. Tyagi, *Introduction to Semiconductor Materials and Devices* (John Wiley & Sons, 2008).
[30]J. H. Davies, *The Physics of Low-Dimensional Semiconductors: An Introduction* (Cambridge University Press, 1997).
[31]D. Akinwande, Y. Nishi, and H.-S. P. Wong, IEEE Trans. Electron Devices **55**, 289 (2008).